Hierarchical ensembles of FeCo metal-organic frameworks reinforced nickel foam as an impedimetric sensor for detection of IL-1RA in human samples

作者為 Shyng-shiou Yuan

提交日期: 2023年04月10日 06:54下午 (UTC+0800)
作業提交代碼: 2060465040
文檔名稱: Chemical_Engineering_Journal,_2023,_458,_141444.pdf (4.77M)
文字總數: 9426
字符總數: 51798

Chemical Engineering Journal 458 (2023) 141444

Contents lists available at ScienceDirect

Chemical Engineering Journal

journal homepage: www.elsevier.com/locate/cej

Hierarchical ensembles of FeCo metal-organic frameworks reinforced nickel foam as an impedimetric sensor for detection of IL-1RA in human samples

Priya Vijayaraghavan [a,1], Yen-Yun Wang [b,c,1], Sathyadevi Palanisamy [d], Li-Yun Lee [d], Yuk-Kwan Chen [b], Shey-Cherng Tzou [d], Shyng-Shiou F. Yuan [a,e,*], Yun-Ming Wang [d,f,*]

[a] Graduate Institute of Medicine, Kaohsiung Medical University, Kaohsiung 807, Taiwan
[b] College of Dental Medicine, Kaohsiung Medical University, Kaohsiung 807, Taiwan
[c] Department of Medical Research, Kaohsiung Medical University Hospital, Kaohsiung 807, Taiwan
[d] Institute of Molecular Medicine and Bioengineering, Center for Intelligent Drug Systems and Smart Bio-devices (IDS^{2}B), National Yang Ming Chiao Tung University, Hsinchu 300, Taiwan
[e] Faculty and College of Medicine, Translational Research Center and Department of Obstetrics and Gynecology, Kaohsiung Medical University, Kaohsiung Medical University Hospital, Kaohsiung 807, Taiwan
[f] Department of Biomedical Science and Environmental Biology, Kaohsiung Medical University, Kaohsiung 807, Taiwan

ARTICLE INFO

Keywords:
Bimetallic MOFs
IL-1RA
Oral cancer
Immunosensor
Clinical analysis

ABSTRACT

Early surveillance of oral cancer demands utmost concern owing to its alarming prevalence in the modern world. An efficient electrochemical impedimetric immunosensor is fabricated based on bimetallic amino-functionalized FeCo metal-organic frameworks uniformly grown on porous nickel foam solid supports (FeCo-MOF@NF) as a transducer for the detection of oral squamous cell carcinoma (OSCC). Herein, the interleukin-1 receptor antagonist (IL-1RA) antibody is used as a biorecognition element for the first time in the determination of oral cancer in real human blood samples using electrochemical impedance spectroscopy (EIS). Furthermore, the presence of specific functional groups ensures selectivity and rapid sensitivity against the target analyte IL-1RA when compared to the other biomarkers including interleukin-6 (IL-6), interleukin-8 (IL-8), CYFRA 21-1, and so on. The immunosensor shows a wide linear dynamic detection range of IL-1RA (10 fg/mL to 10 ng/mL) with a limit of detection (LOD) of 7.30 fg/mL in buffer and 7.22 fg/mL in serum conditions and a limit of quantification (LOQ) of 22.14 fg/mL in PBS and 21.88 fg/mL in serum. For a real-life demonstration, IL-1RA in human samples is detected by the immunosensor for the first time and compared with the gold standard method. The immunosensor also displays an excellent correlation with the standard detection of IL-1RA in human samples. Altogether, this work demonstrates that the electrochemical immunosensor has a high clinical significance by being a promising alternative to conventional approaches.

1. Introduction

Oral cancer is the 6th most common dreadful malignancy, a threatening peril owing to its high death rate and metastasis [1,2]. Every year, oral cancers are estimated to take nearly 128,000 lives, and more than 75 % of fatalities befall in underdeveloped countries [3]. Apart from genetic and environmental factors, it was reported that major causes of oral cancers are due to exposure to tobacco, alcohol, and betel nut chewing in some communities [4–6]. Among several kinds of oral cancers, oral squamous cell carcinoma (OSCC) is the most prevalent [7]. Enormous efforts are devoted to its early screening, diagnosis, and therapy by advanced clinical technologies. Currently, the gold standard approaches to analyze OSCCs are expensive biochemical examinations, and invasive tissue biopsy for histological analysis followed by non-invasive imaging methods including positron emission tomography (PET), computed tomography (CT), magnetic resonance imaging (MRI) [8,9]. The major stumbling block in improving a patient's prognosis is the late detection of the disease. Prevailing diagnostic strategies are not

* Corresponding authors.
E-mail addresses: yuanssf@ms33.hinet.net (S.-S.F. Yuan), ymwang@nycu.edu.tw (Y.-M. Wang).
[1] These authors contributed equally to the paper.

https://doi.org/10.1016/j.cej.2023.141444
Received 7 October 2022; Received in revised form 13 December 2022; Accepted 11 January 2023
Available online 13 January 2023

efficient to detect the disease at a very early stage. On that account, it is highly crucial to develop sensitive and robust techniques for early screening that can significantly contribute to the decrease of mortality.

Biomarkers, the significantly important measurable indicators of biological, pathological and physiological processes, provide useful information for the detection and diagnosis of the disease [1]. Monitoring the biomarkers including DNA, mRNA, proteins, and enzymes also evaluates the pharmacological response to therapy for predicting the prognosis of various diseases, especially cancer [10]. The common biomarkers for oral cancer present in saliva and blood are IL-6, IL-8, CIP2A, CYFRA 21-1, and CD59 [11]. Previously, researchers have detected IL-8 expression in human saliva samples using gold nanoparticles-reduced graphene oxide composite materials which utilize differential pulse voltammetry (DPV) at a detection limit of 72.73 ± 0.18 pg/mL [12]. Another study reports the detection of oral cancer using a CD59 antibody immobilized on a L-cysteine self-assemblies on Au electrodes [13]. Tan et al have adopted a modified approach from traditional DNA biosensors by designing an immobilization-free electrochemical method to target DNA species in oral cancer overexpressed 1 using signal amplification of nicking endonuclease assisted target recycling for the detection of oral cancers in saliva [14]. Ma and Wang's group have demonstrated a versatile ratiomateric DNA biosensor for the detection of oral cancer by integrating homogeneous exonuclease III-assisted target recycling amplification and one-step triggered dual-signal output [15]. A portable electronic biosensor based on reduced graphene oxide (rGO)/melamine (MEL)/antibody/BSA was reported by Ghosh and co-workers for the rapid diagnosis of CEA and CYFRA 21-1 in real-life samples [16].

For successful prediction of specific cancer, multiple biomarkers more than 5 are commonly measured [17]. Hence, the identification of biomarkers may significantly improve the diagnosis and treatment. Interleukin 1 receptor antagonist (IL-1RA), an immunosuppressive cytokine, is an anti-inflammatory protein that counteracts the biological activity of the proinflammatory cytokine, interleukin-1 [18]. Inflammation is associated with early tumor development [19]. Previously, it was also reported that there were elevated levels of IL-1RA in more aggressive OSCCs which can be considered a potential salivary biomarker for the early detection of cancer [18]. In addition, elevated serum levels of IL-1RA were also found in other ailments including rheumatoid arthritis, sepsis, and polymyositis as well as indicating the pathogenesis of schizophrenia [20–22]. Very recent research also contemplated the role of IL-1RA as a plasma biomarker in relapsing-remitting multiple sclerosis [23].

Conventional protein assays such as enzyme-linked immunosorbent assays (ELISAs), gel electrophoresis, mass spectrometry, and fluorescent assays are relatively laborious and time-consuming despite their sensitivity and commercial availability. Furthermore, these techniques have limitations such as high equipment costs and the requirement of highly skilled personnel [12,24]. Therefore, to improve the therapeutic efficiency, it is essential to develop a rapid, ultrasensitive, and dependable electrochemical device for the detection of biomarker proteins in the early stage of oral cancer that can decrease mortality. Compared to the conventional methods for cancer detection, the advantages of electrochemical biosensors include high sensitivity, enhanced selectivity, noninvasive or mildly invasive, and also unhindered by other factors like optical interferences and sample turbidity [11,25,26]. Yet, a sensitive and reliable electrochemical sensor can only be designed by selecting a highly electrically conductive, robust, and biocompatible bioreceptor-transducer matrix.

The emergence of a unique class of porous crystalline materials, metal–organic frameworks (MOFs), also known as porous coordination polymers or inorganic–organic hybrid materials, has demonstrated its potential in numerous areas of research [27]. MOFs consist of metal or metal-cluster secondary building units with polydentate organic bridging ligands [28]. Owing to their large surface area, high pore volume, and presence of tailored –NH_2 and –COOH groups, MOFs are considered to be an exceptional material for the immobilization of protein and other biomolecules [27,29]. Recently MOFs are highly explored as sensitive electrode materials for the trace analysis of biological compounds [30]. Amino-functionalized MOFs have also been reported as highly sensitive and selective fluorescent sensors for DNA [31]. However, poor electron transfer ability and unsteadiness in water are their inherent drawbacks. Hence, MOFs are less explored for electrochemical applications [28]. A significant approach to enhance the use of MOF in sensing applications is to integrate MOF with other tailor-made guest molecules or electrically conducting nanomaterials [32–34]. Introducing bimetallic components in the nodes or secondary building units of metal–organic frameworks could create excessive synergistic effects between the metals [35]. Coupling nonprecious transition metals like Fe and Co into MOFs is known to exert excellent catalytic activities by generating defects and supporting the main catalytic sites of Fe through the conductive networks provided by Co [36,37].

Nickel foam (NF) is an exceptionally unique, interconnected network of porous three-dimensional (3D) material with high surface area and electrical conductivity [38]. There is a wide exploration of NF as a conducting solid substructure to enhance the electrochemical performance of the electrode materials [39,40]. Very recently, Fan and group have fabricated a self-supported binder free glucose sensor using CuO/ZIF-8@NF electrodes [41]. Three dimensional impedimetric immunosensor based on NF along with Au nanoparticles were reported for the detection of sulphate reducing bacteria [42]. Zhang et al. have demonstrated a non-enzymatic detection of glucose using porous $NiMn_2O_4$ nanosheet arrays on NF [43]. The abundant porosity of NF guarantees effective interaction amongst the surface of the conducting materials and electrolytes by boosting the electroactive species and also decreasing the "dead volume" produced by the conducting additives and polymer binders [44,45]. In this context, growing metal–organic frameworks on NF can be considered an efficient way to enhance the electrochemical behavior of electrode materials.

Based on the above-discussed theoretical facts, we have developed a novel electrochemical immunosensor consisting of bimetallic FeCo metal–organic frameworks (FeCo-MOF) supported porous NF (FeCo-MOF/NF) substrates as a transducer material and interleukin-1 receptor antagonist (IL-1RA) as the target for diagnosis of oral cancer using human blood samples. For a healthy adult, the concentrations of IL-1RA range from 100 to 400 pg/mL, whereas patients with oral cancers have been found to have levels exceeding this limit [18,20]. The working electrode, FeCo-MOF/NF was generated by the in-situ hydrothermal synthesis of Fe and Co metal precursors ($FeCl_2{\cdot}4H_2O$ and $Co(NO_3)_2{\cdot}6H_2O$), 2-aminoterephthalic acid ($H_2BDC\text{-}NH_2$), and NF. In the hydrothermal synthesis method, through liquid-phase crystallization and under high pressure, the composition of the single crystals or materials can be regulated with maximum yield and minimal loss. Moreover, this in-situ hydrothermal process is an easy one-step synthesis method that covers synthesis and coating in a single step. It avoids complicated multistep synthesis and different coating procedures. Long-time heating is adapted after several trials with different temperatures and reaction times to achieve uniform growth of the material on the nickel foam. Considering this, the in-situ hydrothermal process ensures a smooth and uniform deposition of the bimetallic MOF in every pore of the nickel foam thereby increasing its immunosensing performance. The synergy between MOFs and NF allows the working electrode to display rapid response, ultrahigh sensitivity, and selectivity owing to the high surface area, improved electron transfer, and high affinity towards biomolecules. The immobilization of anti-IL-1RA antibodies on the working electrode was facilitated via the covalent binding of carboxylic groups and amine groups on the surface of FeCo-MOF/NF. The immunosensor was well characterized by the physicochemical methods including the X-ray diffraction technique (XRD), X-ray photoelectron spectroscopy (XPS), scanning electron microscopy (SEM), and transmission electron microscope (TEM). The changes in the stepwise

modification, and antibody immobilization during electrode fabrication were studied by electrochemical methods. The electrochemical performance of the fabricated immunosensor towards the detection of various concentrations of the target analyte, IL-1RA was successfully demonstrated using electrochemical impedance spectroscopy (EIS). The proposed immunosensor also displayed excellent sensitivity and selectivity in the broad linear range of concentrations. To the best of our knowledge, the present strategy of using hierarchical 3D FeCo-MOF/NF as an electrochemical immunosensor is the first report for utilizing human plasma IL-1RA for the detection of oral cancer in clinical samples. This study provides a new clinically relevant platform for the detection of various disease biomarkers.

2. Experimental section

2.1. Materials

The chemical compounds and reagents used in the study were of analytical grade, purchased commercially and used as received without further purification. Commercial nickel foam, iron (II) chloride tetrahydrate ($FeCl_2{\cdot}4H_2O$), cobalt (II) nitrate hexahydrate ($Co(NO_3)_2{\cdot}6H_2O$), 2-aminoterephthalic acid ($H_2BDC\text{-}NH_2$, greater than 98 wt%) *N*, *N*-dimethylformamide (DMF, 99.5 wt%), ethanol (EtOH, 99.7 %), 2-*N*-morpholinoethanesulfonic acid (MES buffer), 1-ethyl-3-(3-dimethyl aminopropyl)-carbodiimide (EDC), *N*-hydroxysuccinimide (NHS), potassium ferrocyanide ($K_4[(FeCN)_6]$), potassium ferricyanide ($K_3[(FeCN)_6]$), and hexamine ruthenium (III) chloride ($[Ru(NH_3)]Cl_3$) were obtained from Sigma-Aldrich/Merck. Human interleukin-receptor antagonist (IL-1RA) antibody and recombinant human IL-1RA protein were procured from Abcam. Stock solutions of Ab-IL-1RA and Ag-IL-1RA were always freshly prepared in phosphate-buffered saline solution (PBS), pH 7.4. All experiments were conducted at room temperature except as mentioned.

2.2. Fabrication of FeCo-MOF supported on NF electrodes by hydrothermal method

Commercial NF was sliced into pieces of size 3 × 3 cm. The impurities on the NF surface were completely removed by ultrasonication in hydrochloric acid (3 M) for 15 min. In the following step, the acid-treated NF was thoroughly washed with DI water and ethanol. After drying in the oven NF was used for further experiments. The growth of FeCo-MOF nanoarrays on porous NF (labeled as FeCo-MOF/NF) was completed by hydrothermal reaction. The procedure is briefly described here. Typically, a clear solution of $FeCl_2{\cdot}4H_2O$ (0.148 g, 18.6 mM), and $Co(NO_3)_2{\cdot}6H_2O$ (0.218 g, 18.8 mM,) was prepared in dissolving in DMF/ethanol mixture (40 mL). Then $H_2BDC\text{-}NH_2$ (0.271 g, 37.4 mM) was added and continuously stirred until complete dissolution. The resultant solution was carefully transferred into a slantingly placed NF containing Teflon-lined autoclave. A stepwise heating procedure was given for the reaction. Firstly, the stepwise elevation of temperature was attained from 0 °C to 120 °C in 4 h. Then the hydrothermal reaction was continued at 120 °C for 15 h followed by a slow and stepwise cooling for another 12 h. As generated FeCo-MOF/NF was collected into separate containers for washing and subjected to ultrasonication in ethanol and allowed to dry in a vacuum oven at 80 °C. The samples were subjected to structural characterizations including SEM, XRD, TEM, FTIR, and XPS.

2.3. Fabrication of FeCo-MOF/NF electrode with IL-1RA antibody

Biofunctionalization of FeCo-MOF/NF electrodes with IL-1RA antibodies was performed by incubating with fresh solutions of EDC (200 mM, 50 μL), NHS (50 mM, 50 μL) (1:1 v/v in MES buffer) and IL-1RA antibody (0.1 mg/mL, 100 μL,) solution for 4 °C for 1 h. The working areas of FeCo-MOF/NF electrode were dipped inside the solutions and incubated at 4 °C under mild shaking for another 1 h. The resulting IL-1RA antibody-coated FeCo-MOF/NF (FeCo-MOF/NF-IL-1RAAb) was rinsed with Tween 20-PBS solution (0.01 % Tween 20, pH 7.4) to eliminate the unbound molecules. Subsequently, the non-specific antibody sites of the FeCo-MOF/NF-IL-1RAAb electrodes were blocked by incubating with bovine serum albumin (BSA) (0.25 μg/mL, 50 μL) in phosphate-buffered solution (PBS) for 24 h at 4 °C. The bio-functionalized FeCo-MOF/NF-IL-1RAAb-BSA was then refrigerated at 4 °C for future use.

2.4. Collection of human plasma samples

Human plasma samples were obtained from four healthy controls, four oral pre-cancer patients, and four oral cancer patients from Kaohsiung Medical University Hospital, Kaohsiung, Taiwan (ROC). All samples were collected under the protocol approved by the Institutional Review Board (R. No. IRB KMUHIRB-E (1)-20190009) with written consent from the participants. All the samples were collected, processed, and studied under the same criteria. The collected samples were stored in sterilized tubes at −80 °C for future purposes.

2.5. Analysis of human samples

For the electrochemical analysis of human samples, different working concentrations were prepared by diluting 100 μL of human plasma with PBS without carrier protein and incubated at 37 °C for 15 min to facilitate the specific interactions. The IL-1RA in human samples was also analyzed by standard ELISA procedure.

2.6. Characterization

Scanning electron microscopy (SEM), Hitachi S-4800, was used to analyze the morphology of the nanomaterials. Powder X-ray diffractometer (PXRD), Shimadzu XRD-6000, Japan, was used to characterize the crystalline structure and purity of the nanomaterials. High-resolution transmission electron microscopy (HRTEM) was conducted on JEM-2100 at 200 kV. Fourier-transform infrared spectroscopy (FT-IR) was measured in a JASCO FT/IR-460 spectrophotometer in a frequency range of 400–4000 cm^{-1}.

2.7. Electrochemical measurements

Electrochemical impedance spectroscopy (EIS) and cyclic voltammetry (CV) were recorded by an electrochemical analyzer, CH16275D electrochemical workstation with a conventional three-electrode system. A fabricated FeCo-MOF/NF electrode, platinum electrode, and an Ag/AgCl electrode were used as the working electrode, counter electrode, and reference electrode respectively. Antibody immobilized FeCo-MOF/NF electrode was the working electrode; while platinum wire and Ag/AgCl electrode were used as auxiliary and reference electrodes, respectively. EIS experiments was carried out using an equimolar mixture of $K_4[(FeCN)_6]$ (10 mM) and $K_3[(FeCN)_6]$ (10 mM) as the redox probe in PBS buffer. The electrochemical reactions were monitored in the presence of $[Fe(CN)_6]^{3-/4-}$ as the redox couple. CV experiments were conducted using $[Ru(NH_3)_6]Cl_3$ (0.5 mM) and $K_3[(FeCN)_6]$ (0.5 mM) as electrolytes. The various steps monitored in impedance measurements include the fabrication of the immunosensor, biointerfacing the electrode surface with IL-1RA antibody, and IL-1RA antigen detection. The impedance results were represented as Nyquist plots and these plots were recorded in a frequency range of 0.1 Hz to 0.1 MHz at a sinusoidal voltage potential of 0.5 mV. The data is also fitted to an equivalent circuit model to extract the charge transfer resistance (R_{ct}).

3. Results and discussion

3.1. Stepwise fabrication of the impedimetric immunosensor

The bimetallic MOF on Ni Foam was first fabricated by *in situ* hydrothermal processes using ferric chloride, cobalt nitrate, and H_2BDC-NH_2. The formation of MOF-coated NF was first confirmed visually by their color change from silver to brown. Then, FeCo-MOF/NF bioelectrodes were constructed by a stepwise procedure as illustrated in Scheme 1. Initially, the IL-1RA antibody was immobilized covalently on FeCo-MOF/NF using EDC-NHS through a condensation reaction between the carboxylic terminal and the amine terminal of the analyte and FeCo-MOF/NF. After the specific immobilization of the antibody, the non-specific binding of the active sites FeCo-MOF/NF-IL-1RAAb electrodes was intercepted with BSA blocking buffer. The impedimetric immunosensor was now ready for the detection of IL-1RA antigen. A detailed corroboration was achieved by several analytical techniques including SEM, TEM, XRD, XPS, FTIR, and EIS.

3.2. Investigation of structure and morphology of FeCo MOF/NF electrodes

The structural and morphological character of as-synthesized FeCo-MOF/NF were investigated using several techniques including SEM, TEM, XRD, XPS, and FTIR. The surface topography of the FeCo-MOF/NF was analyzed by SEM. The results are depicted in Fig. 1. It revealed the presence of high-yield, uniformly aggregated thin nanosheets protruding outwards from the surface of the NF skeleton. The average thickness of nanosheets was ~ 34–62 nm. To further characterize the materials grown on the NF solid support, a few sheets from the NF surface were scratched off by sonication with ethanol and then analyzed by TEM. The TEM analysis of FeCo-MOF/NF confirmed that the particles formed on the surface have sheet-like structures as shown in Fig. 2. The elemental mapping of FeCo-MOF/NF from TEM-EDX analysis (Fig. 2c) clearly discerns the presence of homogeneously distributed elements including, iron (Fe), cobalt (Co), carbon (C), oxygen (O), and nitrogen (N) on each layer of MOF. From this information, it is confirmed that the material uniformly grown on the NF skeleton is bimetallic FeCo-MOF.

FeCo-MOF grown on Ni foam skeleton has high crystallinity as confirmed by the powder XRD and the simulated XRD pattern (Fig. 3a). A successful immunosensor can only be accomplished by the presence of suitable functional groups on the surface of the materials to facilitate biorecognition. Hence, to confirm various functional groups, present in FeCo-MOF/NF, FTIR analysis was performed. Fig. 3b exhibits the characteristic vibrational frequencies of FeCo-MOF/NF. The peaks at 1410 cm^{-1} and 1590 cm^{-1} can be imputed to the symmetric and asymmetric stretching vibrations of the –COOH. The broad vibrational band appearing at 3100 cm^{-1} to 3500 cm^{-1} specifies the presence of symmetrical and asymmetrical stretching vibrations of $-NH_2$ groups validating the presence of H_2BDC-NH_2 as the ligand for the synthesis of FeCo-MOF/NF. The vibrational bands below 600 cm^{-1} were ascribed to the presence of stretching frequencies of metal-oxo bonds including Co-O and Fe-O. Thus, the successful fabrication of FeCo-MOF/NF was confirmed by FTIR analysis.

To gain a deeper insight into the electronic structure and chemical states of FeCo-MOF/NF, XPS analysis was performed. Fig. 4a displays the wide scan XPS spectra of FeCo-MOF/NF indicating the clear presence of Ni, Fe, Co, O, C, and N. Needless to say, the characteristic information obtained from the XPS analysis and TEM-EDX mapping is undoubtedly consistent with each other. The deconvoluted high resolution spectrum of each element is portrayed in Fig. 4b–f. The high-resolution XPS spectrum of Fe 2p displayed two major binding energies at 724.6 eV, 711.5 eV, and shakeup satellite peaks at 717–722 eV representing $2p_{1/2}$ and $2p_{3/2}$ (Fig. 4b) [46]. The binding energies of

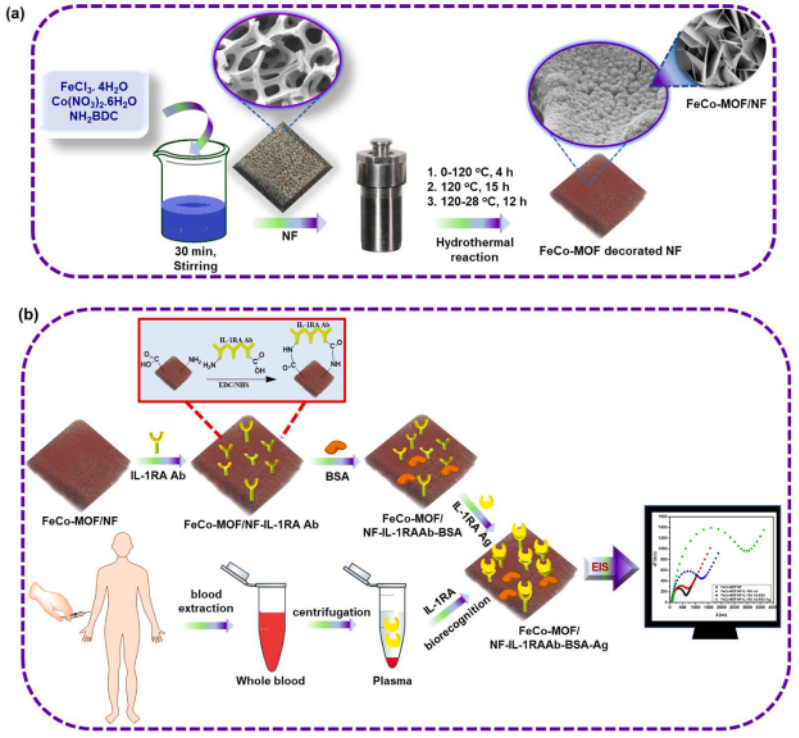

Scheme 1. Schematic illustration of(a) the synthesis of FeCo-MOF/NF and (b) immunosensor fabrication for clinical detection of IL-1RA.

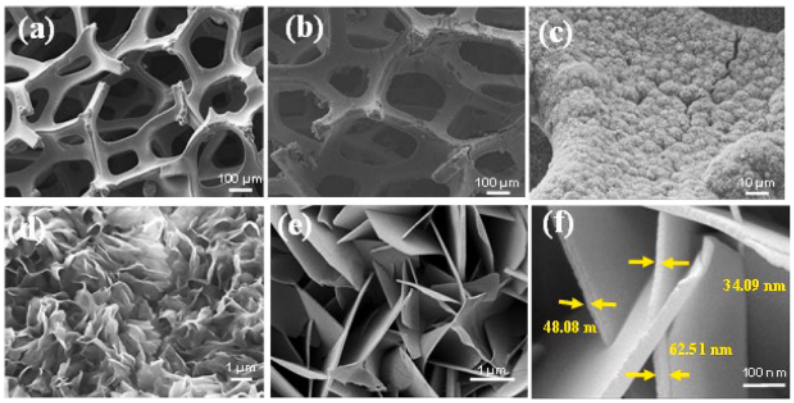

Fig. 1. (a) SEM images of bare porous NF, (b-f) FeCo-MOF grown on NF skeleton (FeCo-MOF/NF) after *in situ* hydrothermal reactions using precursors, ligands, and Ni foam skeleton under different magnification. The markings in f) are the average thickness of FeCo-MOF nanosheets grown on porous NF supports.

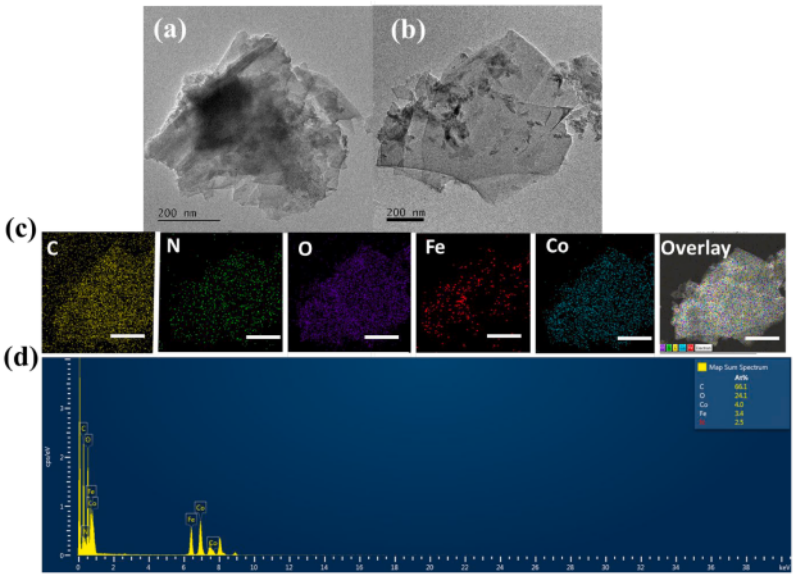

Fig. 2. (a, b) TEM images of a thin section of FeCo-MOF scratched from NF skeleton after *in situ* hydrothermal reactions using metal precursors, ligands, and NF, (c, d) TEM-EDX mapping images and EDX spectra of FeCo-MOF, respectively. Scale bar:100 nm.

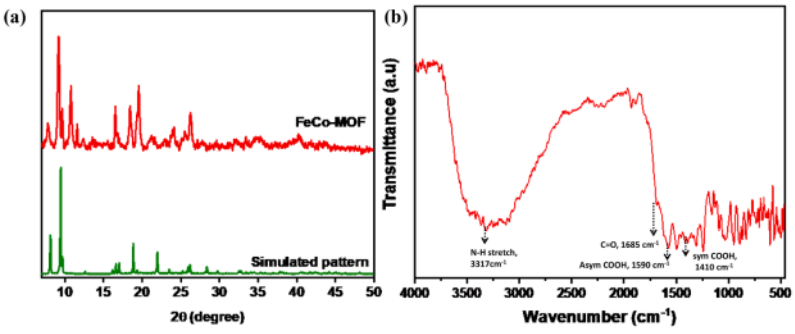

Fig. 3. (a) Powder XRD pattern with the simulated report of FeCo-MOF scratched from Ni foam surface and (b) FTIR images of FeCo-MOF/NF.

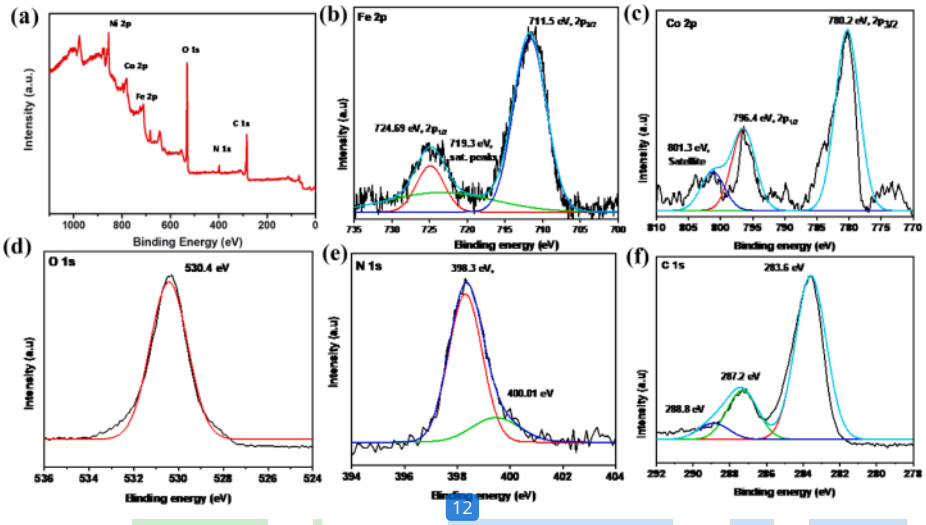

Fig. 4. (a) Full range XPS survey scan of FeCo-MOF/NF, (b-f) deconvoluted high-resolution XPS spectra of Fe 2p, Co 2p, Oo 1s, N 1s, and C 1s, respectively.

Co $2p_{3/2}$ and $2p_{1/2}$ were found at 780.2 and 79[illegible] eV, respectively (Fig. 4c) validating the Co^{2+} oxidation state [47]. In addition, the C 1s spectrum is deconvoluted to three peaks at 283.2, 287.2, and 288.4 eV representing C—C, C—O, and C═O bonds, respectively [47]. Correspondingly, N 1s exhibited two peaks at 398.3 and 400.0 eV associated with the amine and nitrogen, respectively. Oxygen 1s spectrum also showed a broad binding energy peak at 530.4 eV.

3.3. Immunosensor fabrication

To facilitate the biorecognition of IL-1RA, FeCo-MOF/NF was covalently modified with anti-IL-1RA by EDC-NHS coupling. Every layer of fabrication, including the successful conjugation of the sensing element on FeCo-MOF/NF and antigen recognition, was primarily confirmed by a surface analysis using SEM and chemically analyzed by FTIR spectroscopy. Fig. S2 confirms the morphological alterations on the surface of the FeCo-MOF/NF immunosensor after each step of fabrication. A typical high magnification SEM image of FeCo-MOF/NF shows the presence of fully aggregated sheet-like morphology (Fig. S2a). As the antibody was immobilized onto the nickel foam electrodes there is an obvious variation in the morphology exposing a flocculant globular structure of the proteins on the surface (Fig. S2b). Further, the nonspecific adsorption of BSA appeared as a layered hazy structure on the surface of the electrodes (Fig. S2c). The IL-1RA antigen-specific immune interaction was also confirmed by SEM images in Fig. S2d, by the appearance of flocculant coating on the surface. Cross-sectional SEM analysis for the determination of the thickness of the immunosensor during each step of fabrication including pristine NF, FeCo-MOF/NF, FeCo-MOF/NF-IL-1RAAb, FeCo-MOF/NF-IL-1RAAb-BSA, and FeCo-MOF/NF-IL-1RAAb-BSA-Ag was also conducted (Fig. S3). The average thickness of Ni foam was found to be 0.71 mm. The thickness of FeCo MOF/NF deposition over the layer was approximately 6.19 μm. Further, each new layer in the fabrication of the immunosensor resulted in an increase of the thickness from 7.61 μm to 14.46 μm above Ni foam.

The information gained from SEM was further chemically validated by EDS mapping and FTIR spectroscopy in Figs. S4 and S5, respectively. To evaluate the coverage of IL-1RA, EDS elemental analysis of FeCo-MOF/NF was performed during every step of fabrication. The results displayed in Fig. S4 are EDS mapping images with corresponding elemental composition. The results confirmed the presence of carbon, oxygen, nitrogen, iron, and cobalt. It is also displayed that after each step of immunosensor fabrication, the increase in elemental percentage confirmed that overall protein coating has been increased. This confirms the successful fabrication of the immunosensor and also provides strong evidence for the extensive coverage of IL-1RA over FeCo-MOF/NF electrodes.

Further, the successful covalent immobilization of anti-IL-1RA on FeCo-MOF/NF was revealed by the appearance of representative peaks for amide C—N stretching (1232 cm^{-1}), amide N—H (1534 cm^{-1}), amide C—O bond (1628 cm^{-1}), and amide NH_2 stretching 3302 cm^{-1} (Fig. S5). Moreover, the intensity of C—N stretching vibrations (1232 cm^{-1}) with every layer of a modification indicates the successful fabrication of the bioelectrodes. All these corroborations further encouraged to proceed toward the electrochemical studies of the immunosensor for the biorecognition of IL-1RA.

3.4. Electrochemical analysis

Aiming to investigate the electrochemical performance of the immunosensor, the EIS, a highly sensitive and powerful technique, was employed towards recognizing the specific target IL-1RA. In EIS, the electron transfer kinetics at every layer of modification of the immunosensor was monitored by the change in the real part, charge transfer resistance (R_{ct}), of the electrode impedance in a way of graphical representation known as Nyquist's plots. As the impedimetric expressions consist of two components, real and imaginary, the arc or straight line obtained in Nyquist's plots is the impedance value gained by plotting the real part (Z', in-phase) against the imaginary part (Z'', out-of-phase) at various frequencies. Impedimetric sensors are classified into two types, Faradaic and non-Faradaic. Since, the Faradaic mode utilizes electrochemical redox reactions to produce impedance, in general, for the quantitative analysis of biorecognition events Faradaic mode offers more versatility. Variations in the R_{ct} are observed when the Faradaic mode is hampered by the antibody-antigen interactions catalyzing the redox probe. The decrease in the R_{ct} value indicates a rapid rate of electron transfer among the electrodes and electrolytes. The experimental R_{ct} values obtained from the EIS measurements were fitted with Randle's equivalent circuit model.

Fig. 5 shows the impedimetric characterization of the layer-by-layer fabrication of the immunosensor FeCo-MOF/NF, FeCo-MOF/NF-IL-1RAAb, FeCo-MOF/NF-IL-1RAAb-BSA, and FeCo-MOF/NF-IL-1RAAb-BSA-Ag electrodes. The impedance spectra were measured based on redox reactions of $[Fe(CN)_6]^{3-/4-}$ electrolyte and fitted with equivalent Randle's circuit (inset in Fig. 5). The R_{ct} values were found to be 390.7,

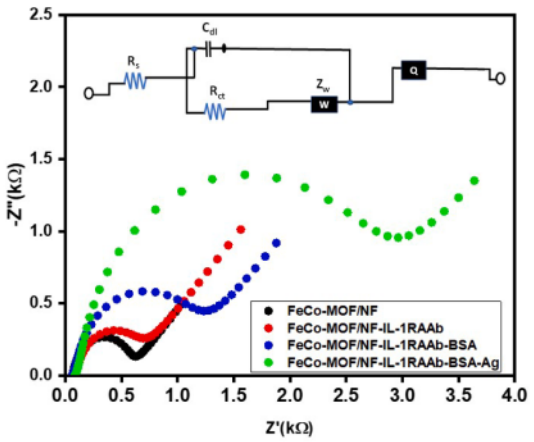

Fig. 5. Impedimetric characterization of the fabrication of the FeCo-MOF/NF immunosensor for IL-1RA detection in 10 mM $K_3[Fe(CN_6)]/K_4[Fe(CN_6)]$ by EIS. Inset: equivalent circuit diagram for fitting the impedimetric detection of IL-1RA. R_s, R_{ct}, Z_w, Q, and C_{dl} symbolize the solution resistance, charge transfer impedance, Warburg impedance, constant phase element, and double-layer capacitance, respectively.

465.9, 913.3, and 2898 kΩ for FeCo-MOF/NF-IL-1RAAb-BSA-Ag, FeCo-MOF/NF-IL-1RAAb-BSA, FeCo-MOF/NF-IL-1RAAb, FeCo-MOF/NF electrodes, respectively. Step-wise fabrication of the immunosensor with new layers was witnessed with an increase in the charge transfer resistance (R_{ct}) value. It can be observed that the R_{ct} value of the FeCo-MOF/NF electrode is very low. The low value of R_{ct} is attributed to the rapid diffusion of charge from the redox probe owing to the hindrance-free accessibility of the electrode surface. This suggests the appropriateness of the FeCo-MOF/NF electrode for further modification. After the covalent conjugation with the IL-1RA antibody, the R_{ct} value of FeCo-MOF/NF-IL-1RAAb was found to be increased. The immobilization of antibodies on the surface of the electrode introduced an electrical barrier layer that hindered the smooth diffusion of the electrical charge on the electrode surface. Further modification of the electrode surface by the nonspecific binding of BSA resulted in a noticeably higher impedance peak for the FeCo-MOF/NF-IL-1RAAb-BSA electrode apparently due to the insulating nature of BSA on the electrolyte and electrode surface. The antigen-specific sensing by FeCo-MOF/NF immunosensor when exposed to the target protein IL-1RA, displayed a higher R_{ct} value as compared with other electrodes, confirming the specificity of the immunosensor.

To investigate the electrochemical properties of the sensor, redox probes with different charges were employed to identify the changes in the electrode surface exposed to antigens (Fig. S6). The peak current of the negatively charged redox mediator potassium ferricyanide, $K_3[Fe(CN)_6]$ showed minor changes whereas the peak current of the positively charged redox probe, hexaammineruthenium(III) chloride, $[Ru(NH_3)_6]Cl_3$ is found to be increased when treated with 10 ng/mL of antigen. These results indicate that the response of the sensors resulted from the change of the charge at the electrode interface.

3.5. Quantitative detection of IL-1RA antigen using the proposed immunosensor

One of the main goals of this study is to establish an immunosensor with high sensitivity even at low concentrations in human blood samples. Due to the presence of interfering components in blood samples that may interfere with the biorecognition, parallel studies were conducted in PBS and 10 % serum. The electrochemical performance of FeCo-MOF/NF-IL-1RAAb immunosensor was analyzed by detecting appropriate concentrations of IL-1RA in a wide range varying from 10 ng/mL to 10 fg/mL in both buffered and saline solutions. The measurements were triplicated under the same conditions. The results of the analytical ability of the immunosensor were detected by the variations in charge transfer resistance based on the impedance and displayed as Nyquist plots as shown in Fig. 6a and c.

According to the results obtained from the Nyquist plot, it is evident that there is a steady increase in the value R_{ct} towards the higher concentration of IL-1RA. The increase in the R_{ct} can be attributed to the restricted electrostatic interaction between the analyte and electrolyte during the biorecognition events of the immunocomplex. Increasing the analyte layering resulted in introducing a major kinetic barrier for the active charge transfer and facile electrolyte diffusion on the electrode surface. Furthermore, the increase in the concentration of the immune complex effectively hindered the unrestricted accessibility of the free area of the working electrode. FeCo-MOF/NF-IL-RA immunosensor also presented a linear response in the determination of the IL-RA analyte (Fig. 6b and d) with a coefficient of determination in the linear regression equation, (R^2) as 0.9904 and 0.9938 in PBS and serum solutions, respectively. Values of R_{ct} and solution resistance R_s are displayed in Table S1.

The limit of detection (LOD) of the immunosensor was determined using the formula:

$$LOD = \frac{3.3\sigma}{} \quad (1)$$

and limit of quantification (LOQ) was calculated using the formula:

$$LOQ = \frac{10\sigma}{S} \quad (2)$$

where 'σ' is the standard deviation and 'S' is the slope of the curve. On account of these parameters, the LOD value of FeCo-MOF/NF-IL-1RA immunosensor was obtained as 7.30 fg/mL and 7.22 fg/mL in PBS and serum conditions, respectively. The calculated LOQ value for the immunosensor was 22.14 fg/mL in PBS and 21.88 fg/mL serum, respectively.

The exceptionally high sensitivity of the IL-1RA immunosensor was clearly indicated here when compared to other reported oral cancer biomarkers (Table 1). The rapid and ultra-high sensitivity of the immunosensor towards IL-1RA thus assured that the sensor could be utilized for the analysis of human blood samples.

3.6. Selectivity, stability, reusability, and reproducibility of the immunosensor

Prior to the human sample analysis, a dependable immunosensor must also be tested for its selectivity, stability, reusability, and reproducibility. Human plasma contains numerous other analytes that may interfere with the assessment of the biomarker. Therefore, FeCo-MOF/NF-IL-1RAAb BSA bioelectrodes were further analyzed for their specificity toward the biorecognition of IL-1RA antigen. The immunosensor was exposed to other oral cancer biomarkers like basic fibroblast growth factor (bFGF), interferon-gamma (IFN-γ), granulocyte macrophage-colony stimulating factor (GM-CSF), osteopontin, and urokinase-type plasminogen activator receptor (uPAR), interleukin-6 (IL-6), interleukin-8 (IL-8), and CYFRA 21-1. Each of these interferants was exposed to FeCo-MOF/NF-IL-1RAAb-BSA bioelectrode with a concentration of 10 ng/mL and subjected to EIS measurements. The highly specific behavior of the proposed immunosensor towards the target analyte, IL-1RA is depicted in Fig. 7a. Evidently, the immunosensor FeCo-MOF/IL-1RAAb-BSA, revealed minor sensitivity towards other biomarkers when compared to IL-1RA antigen.

The physical, chemical, and mechanical stability of the immunosensor were evaluated by exposing it to various conditions including pH (acidic, neutral, and basic), temperature (37 °C and 4 °C), and ultrasonication. Fig. S7 displays the morphological stability of the

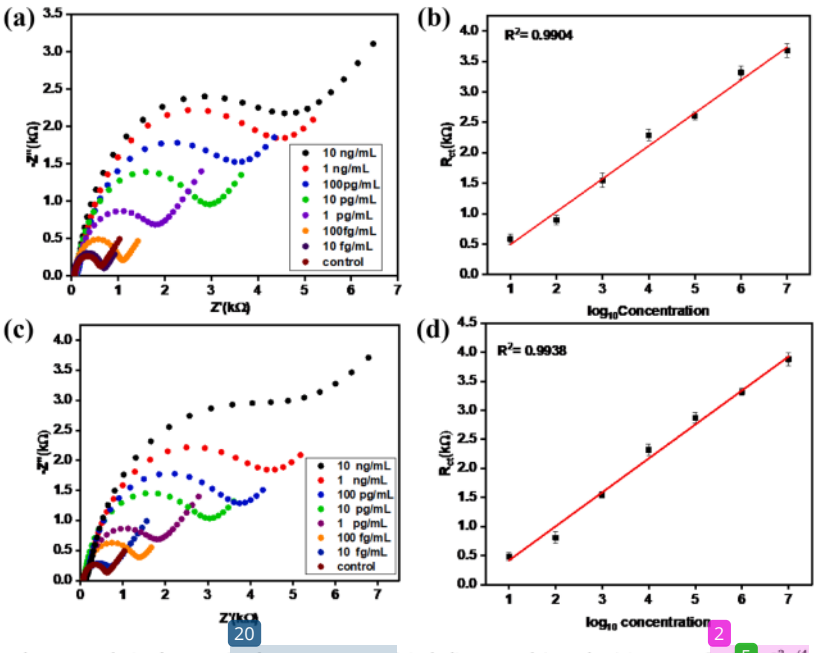

Fig. 6. Concentration-dependent EIS analysis of IL-1RA (10 fg/mL to 10 ng/mL) including control (zero-dose) in 10 mM $[Fe(CN)_6]^{3-/4-}$ as a redox probe. Nyquist plots of concentration-dependent response studies in (a) buffer and (c) serum solutions. (b) and (d) Calibration plot of IL-1RA in the linearity range 10 fg/mL to 10 ng/mL in buffer and serum solutions, respectively.

Table 1
List of previously reported biosensors for oral cancer (CV = cyclic voltammetry, SWV = square wave voltammetry, A = Amperometry).

S.No.	Immunosensor matrix	Analyte	LOD	Method	Ref.
1	Anti-IL8/AuNPs-rGO/ITO	IL8	72.4 pg/mL (in saliva) 72.73 pg/mL (in buffer)	DPV	[12]
2	/cysteine/anti-CD59	CD59	0.84 fg/mL	EIS	[13]
3	Anti-CYFRA-21–1/APTES/ZrO_2/ITO	CYFRA 21–1	0.08 ng/mL	CV	[49]
4	Gold/MCH/signaling probe T1 electrode	DNA	0.02 fM	A	[50]
5	Anti-IL6/SWNTs/graphite	IL6	0.5 pg/mL (in calf serum)	A	[51]
6	Anti-CEA/MWCNT-PEI/SPE	CEA	1×10^{-12} g/mL	SWV	[52]
7	FeCo-MOF/NF-IL-1RAAb	IL-1RA	7.30 fg/mL (buffer) 7.22 fg/mL (serum)	EIS	Present work

immunosensor subjected to different conditions including pH = 5 and 10 solutions, temperature, and ultrasonication. As shown in the high magnification SEM images there is no evident perturbation in the morphology of FeCo-MOF/NF under acidic and various thermal conditions. In contrast, exposing the immunosensor to basic conditions (pH = 10) displayed a slight change in morphology by the formation of spherical particles. This slight variation in morphology of FeCo-MOF in alkaline solutions may be attributed to the rapid hydrolysis of the MOF owing to the partial substitution of Co by OH^- ions from the much weaker Co-O bonds compared to Fe-O bonds [48]. However, this morphological change did not show any interference in the electrochemical behavior of the immunosensor. The EIS measurements for the immunosensor denoted a similar sensitivity for the immunosensor when subjected to different conditions of pH and temperature (Fig. S8a and b). The stability of the immunosensor was evaluated after exposing the sensor to the open air for 6 days under humid conditions (relative humidity of 45 %) (Fig. S8c). The sensor was stable for 4 days after being coated with the biomolecule. After 4 days there was a decrease in the signal and a total loss of signal was observed on the 5th day. FeCo-MOF/NF immunosensor was also exposed to different biological buffers including PBS, Tris, and MES. The results are displayed in Fig. S9. As seen from the results buffer significantly affected the performance of the sensor by changing the EIS output of FeCo-MOF/NF-IL-1RAAb-BSA-Ag due to the difference in their pH conditions.

To ensure the reproducibility of the immunosensor, three different batches of identically synthesized electrodes were used to detect three concentrations (1 pg/mL, 1 ng/mL, and 10 ng/mL) of IL-1RA antigen. The results are displayed in Fig. 7b. The R_{ct} values of the immunosensor revealed an identical response to the analyte IL-1RA antigen, suggesting that the immunosensor shows excellent reproducibility. The reusability of the immunosensor was investigated under optimum conditions (Fig. S10). The impedimetric signals started gradually decreasing after every reuse. The immunosensor displayed a total loss of signal during the 5th cycle displaying only 4.6 % of the initial value.

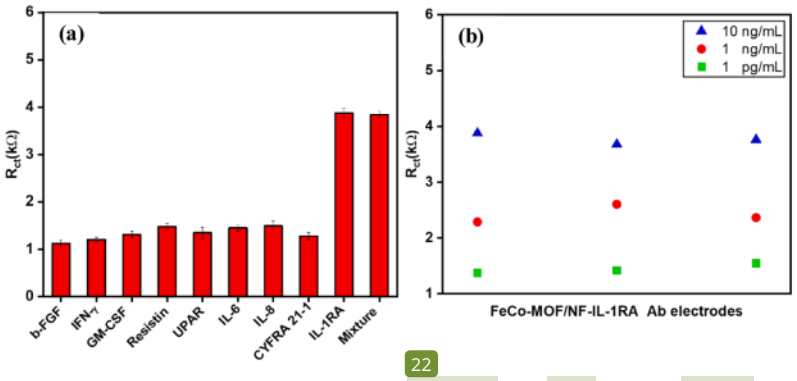

Fig. 7. (a) specificity of feco-mof/nf-il-1raab-bsa immunosensor towards b-fgf (10 ng/mL), IFN-γ (10 ng/mL), GM-CSF (10 ng/mL), Resistin (10 ng/mL), UPAR (10 ng/mL), IL-6 (10 ng/mL), IL-8 (10 ng/mL), CYFRA 21-1 (10 ng/mL), IL-1RA (10 ng/mL), and mixture of antigens. (b) Impedimetric response of three different batches of FeCo-MOF/NF-IL-1RAAb-BSA immunosensor detecting three different concentrations of IL-1RA (10 ng/mL, 1 ng/mL, and 1 pg/mL).

Table 2
Analytical results of IL-1RA in human plasma samples from oral cancer and precancer patients as well as healthy controls.

Patient No.	Classification	IL-1RA (pg/mL) (ELISA)	RSD (%)	IL-1RA (pg/mL) (EIS)	RSD (%)
1	Normal	2.5	22.32	3.07	5.71
2		381	2.11	330.71	0.88
3		2.5	12.38	2.72	19.63
4		3.8	5.52	70.44	4.01
5	Pre-cancer	undetectable	–	0.001	5.47
6		2273	0.23	691.81	13.43
7		2.5	21.16	1.58	16.21
8		7.5	7.37	6.30	11.95
9	Cancer	653	2.9	398.10	5.13
10		undetectable	–	0.95	16.38
11		undetectable	–	0.09	12.06
12		undetectable	–	0.19	13.41

3.7. Detection of IL-1RA in human blood samples

In order to demonstrate the potential clinical application of the proposed immunosensor, concentrations of IL-1RA in human samples were estimated in four healthy controls, four pre-cancer patients, and four oral cancer patients. The results were also compared with the gold standard enzymatic assay ELISA. The results are displayed in Table 2. As shown, there is a reasonable correlation between the concentrations of IL-1RA obtained from the proposed immunosensor by the EIS method and ELISA. The values of relative standard deviation (RSD) were acceptable indicating the potential accuracy of the proposed immunosensor. In previous reports, the plasma and salivary levels of IL-1RA were elevated in oral cancer patients of Sweden and Saudi Arabia respectively, compared to healthy controls [18,53]. However, in this study, we did not observe elevated plasma IL-1RA levels in oral precancer and cancer patients (Table 2). Since the etiology in these two countries is mostly HPV-related while it is mostly areca nut-related in Taiwanese patients, it is possible that different carcinogens may have a different effect in promoting IL-1RA expression. Besides, it is encouraging to notice the ultra-high sensitivity of the impedimetric sensor to detect such a low level of IL-1RA that were not detectable by ELISA measurements.

Moreover, considering the potent role of IL-1RA as a biomarker for many chronic and progressively fatal disorders, the sensing characteristics of the current immunosensor can also be assured for the detection of diseases other than oral cancer with ultra-high sensitivity and specificity even at very low concentrations. In near future, we anticipate to perform the biorecognition of IL-1RA with the proposed immunosensor from the clinical samples in a more appropriate medium, like saliva or tissues.

4. Conclusions

This study demonstrates the fabrication of a hierarchically grown three-dimensional amino functionalized FeCo-MOF on Ni foam solid substrates, FeCo-MOF/NF, for ultrahigh sensitive detection of IL-1RA in human samples as a biomarker for oral cancer using electrochemical impedance spectroscopy. FeCo-MOF was hydrothermally synthesized in the presence of Ni foam and successfully immobilized IL-1RA antibodies for the biorecognition of the target analyte. FeCo-MOF/NF bio-electrodes show high sensitivity and rapid detection with a wide linear range of 10 fg/mL to 10 ng/mL. The detection limit was 7.30 fg/mL and 7.22 fg/mL in buffer and 10 % serum solutions. The limit of quantification (LOQ) of the immunosensor was determined to be 22.14 fg/mL in PBS and 21.88 fg/mL in serum. The proposed immunosensor also displayed excellent sensitivity toward IL-1RA antigen in human plasma samples. Consequently, demonstrating an innovative way of detecting disease markers by coupling the impedimetric immunosensor FeCo-MOF/NF and antibodies broadens new avenues for sustainable diagnostic tools in the near future.

Declaration of Competing Interest

The authors declare that they have no known competing financial interests or personal relationships that could have appeared to influence the work reported in this paper.

Data availability

Data will be made available on request.

Acknowledgements

The authors want to gratefully thank the financial supports by the National Science and Technology Council NSTC110-2113-M-A49-003, the "Center for Intelligent Drug Systems and Smart Bio-devices (IDS^2B)" and "Smart Platform of Dynamic Systems Biology for Therapeutic Development" project from The Featured Areas Research Center Program within the framework of the Higher Education Sprout Project by the Ministry of Education (MOE) in Taiwan. This work was also funded by the Higher Education Sprout Project of the National Yang Ming Chiao Tung University and Ministry of Education (MOE) and in part supported by the National Yang Ming Chiao Tung University-

Kaohsiung Medical University joint research project (#NYCU-KMU-111-I002) from Taiwan.

Appendix A. Supplementary data

Supplementary data to this article can be found online at https://doi.org/10.1016/j.cej.2023.141444.

References

[1] T. Radhika, N. Jeddy, S. Nithya, R.M. Muthumeenakshi, Salivary biomarkers in oral squamous cell carcinoma – an insight, J. Oral Biol. Craniofac Res. 6 (Suppl 1) (2016) S51–S54, https://doi.org/10.1016/j.jobcr.2016.07.003.

[2] Z. Khurshid, M.S. Zafar, R.S. Khan, S. Najeeb, P.D. Slowey, I.U. Rehman, Role of salivary biomarkers in oral cancer detection, Adv. Clin. Chem. 86 (2018) 23–70, https://doi.org/10.1016/bs.acc.2018.05.002.

[3] A. Jemal, F. Bray, M.M. Center, J. Ferlay, E. Ward, D. Forman, Global cancer statistics, CA Cancer J. Clin. 61 (2011) 69–90, https://doi.org/10.3322/caac.20107.

[4] S.L. Chuang, W.W. Su, S.L. Chen, A.M. Yen, C.P. Wang, J.C. Fann, S.Y. Chiu, Y. C. Lee, H.M. Chiu, D.C. Chang, Y.Y. Jou, C.Y. Wu, H.H. Chen, M.K. Chen, S. T. Chiou, Population-based screening program for reducing oral cancer mortality in 2,334,299 Taiwanese cigarette smokers and/or betel quid chewers, Cancer 123 (2017) 1597–1609, https://doi.org/10.1002/cncr.30517.

[5] M. Kumar, R. Nanavati, T.G. Modi, C. Dobariya, Oral cancer: etiology and risk factors: A review, J. Cancer Res. Ther. 12 (2016) 458–463, https://doi.org/10.4103/0973-1482.186696.

[6] A.M. Yen, S.C. Chen, T.H. Chen, Dose-response relationships of oral habits associated with the risk of oral pre-malignant lesions among men who chew betel quid, Oral Oncol. 43 (2007) 634–638, https://doi.org/10.1016/j.oraloncology.2006.05.001.

[7] S. Hu, M. Arellano, P. Boontheung, J. Wang, H. Zhou, J. Jiang, D. Elashoff, R. Wei, J.A. Loo, D.T. Wong, Salivary proteomics for oral cancer biomarker discovery, Clin. Cancer Res. 14 (2008) 6246-6252. 10.1158/1078-0432.Ccr-07-5037.

[8] S. Kantola, M. Parikka, K. Jokinen, K. Hyrynkangs, Y. Soini, O.P. Alho, T. Salo, Prognostic factors in tongue cancer - relative importance of demographic, clinical and histopathological factors, Br. J. Cancer 83 (2000) 614–619, https://doi.org/10.1054/bjoc.2000.1323.

[9] R. Sannam Khan, Z. Khurshid, S. Akhbar, S. Faraz Moin, Advances of salivary proteomics in oral squamous cell carcinoma (OSCC) detection: an update, Proteomes 4 (2016), https://doi.org/10.3390/proteomes4040041.

[10] L. Wu, X. Qu, Cancer biomarker detection: recent achievements and challenges, Chem. Soc. Rev. 44 (2015) 2963–2997, https://doi.org/10.1039/C4CS00370E.

[11] Y.T. Lin, S. Darvishi, A. Preet, T.Y. Huang, S.H. Lin, H.H. Girault, L. Wang, T.E. Lin, A review: electrochemical biosensors for oral cancer, Chemosensors 8 (2020) 54.

[12] S. Verma, A. Singh, A. Shukla, J. Kaswan, K. Arora, J. Ramirez-Vick, P. Singh, S. P. Singh, Anti-IL8/AuNPs-rGO/ITO as an Immunosensing platform for noninvasive electrochemical detection of oral cancer, ACS Appl. Mater. Interfaces 9 (2017) 27462–27474, https://doi.org/10.1021/acsami.7b06839.

[13] M. Choudhary, P. Yadav, A. Singh, S. Kaur, J. Ramirez-Vick, P. Chandra, K. Arora, S.P. Singh, CD 59 Targeted ultrasensitive electrochemical immunosensor for fast and noninvasive diagnosis of oral cancer, Electroanalysis 28 (2016) 2565–2574, https://doi.org/10.1002/elan.201600238.

[14] Y. Tan, X. Wei, M. Zhao, B. Qiu, L. Guo, Z. Lin, H.-H. Yang, Ultraselective homogeneous electrochemical biosensor for DNA species related to oral cancer based on nicking endonuclease assisted target recycling amplification, Anal. Chem. 87 (2015) 9204–9208, https://doi.org/10.1021/acs.analchem.5b01470.

[15] R.-N. Ma, L.-L. Wang, H.-F. Wang, L.-P. Jia, W. Zhang, L. Shang, Q.-W. Xue, W.-L. Jia, Q.-Y. Liu, H.-S. Wang, Highly sensitive ratiometric electrochemical DNA biosensor based on homogeneous exonuclease III-assisted target recycling amplification and one-step triggered dual-signal output, Sens. Actuators B Chem. 269 (2018) 173–179, https://doi.org/10.1016/j.snb.2018.04.143.

[16] S. Joshi, S. Kallappa, P. Kumar, S. Shukla, R. Ghosh, Simple diagnosis of cancer by detecting CEA and CYFRA 21–1 in saliva using electronic sensors, Sci. Rep. (2022) 15315.

[17] A.D. Weston, L. Hood, Systems biology, proteomics, and the future of health care: toward predictive, preventative, and personalized medicine, J. Proteome Res. 3 (2004) 179–196, https://doi.org/10.1021/pr0499693.

[18] S. Aziz, S.S. Ahmed, A. Ali, F.A. Khan, G. Zulfiqar, J. Iqbal, A.A. Khan, M. Shoaib, Salivary immunosuppressive cytokines IL-10 and IL-13 are significantly elevated in oral squamous cell carcinoma patients, Cancer Invest. 33 (2015) 318–328, https://doi.org/10.3109/07357907.2015.1041642.

[19] M. Shiiba, K. Saito, H. Yamagami, D. Nakashima, M. Higo, A. Kasamatsu, Y. Sakamoto, K. Ogawara, K. Uzawa, Y. Takiguchi, H. Tanzawa, Interleukin-1 receptor antagonist (IL1RN) is associated with suppression of early carcinogenic events in human oral malignancies, Int. J. Oncol. 46 (2015) 1978–1984, https://doi.org/10.3892/ijo.2015.2917.

[20] C.A. Meier, E. Bobbioni, C. Gabay, F. Assimacopoulos-Jeannet, A. Golay, J.-M. Dayer, IL-1 receptor antagonist serum levels are increased in human obesity: a possible link to the resistance to leptin? J. Clin. Endocrin. Metab. 87 (3) (2002) 1184–1188.

[21] Y. Lin, Y. Peng, S. He, J. Xu, Y. Shi, Y. Su, C. Zhu, X. Zhang, R. Zhou, D. Cui, Serum IL-1ra, a novel biomarker predicting olanzapine-induced hypercholesterolemia and hyperleptinemia in schizophrenia, Prog. Neuropsychopharmacol. Biol. Psychiatry 84 (2018) 71–78, https://doi.org/10.1016/j.pnpbp.2018.01.020.

[22] W.P. Arend, M. Malyak, C.J. Guthridge, C. Gabay, Interleukin-1 receptor antagonist: role in biology, Annu. Rev. Immunol. 16 (1998) 27–55, https://doi.org/10.1146/annurev.immunol.16.1.27.

[23] S.N. Blandford, D.A. Galloway, J.B. Williams, S. Arsenault, J. Brown, G. MacLean, G.R.W. Moore, J. Barron, M. Ploughman, F. Clift, M. Stefanelli, C.S. Moore, Interleukin-1 receptor antagonist: An exploratory plasma biomarker that correlates with disability and provides pathophysiological insights in relapsing-remitting multiple sclerosis, Mult. Scler. Relat. Disord. 52 (2021), 103006, https://doi.org/10.1016/j.msard.2021.103006.

[24] P.H. Montero, S.G. Patel, Cancer of the oral cavity, Surg. Oncol. Clin. N. Am. 24 (2015) 491–508, https://doi.org/10.1016/j.soc.2015.03.006.

[25] S. Mishra, D. Saadat, O. Kwon, Y. Lee, W.S. Choi, J.H. Kim, W.H. Yeo, Recent advances in salivary cancer diagnostics enabled by biosensors and bioelectronics, Biosens. Bioelectron. 81 (2016) 181–197, https://doi.org/10.1016/j.bios.2016.02.040.

[26] X.-J. Chen, X.-Q. Zhang, Q. Liu, J. Zhang, G. Zhou, Nanotechnology: a promising method for oral cancer detection and diagnosis, J. Nanobiotechnol. 16 (2018) 52, https://doi.org/10.1186/s12951-018-0378-6.

[27] R. Liu, L. Ran, B. Niu, Y. Wei, Carbonization of Fe-based metal organic frameworks with mesoporous structure as electrocatalyst for catalysis of oxygen to hydrogen peroxide, J. Nanosci. Nanotechnol. 18 (2018) 4667–4674, https://doi.org/10.1166/jnn.2018.15311.

[28] Y. Bai, Y. Dou, L.-H. Xie, W. Rutledge, J.-R. Li, H.-C. Zhou, Zr-based metal–organic frameworks: design, synthesis, structure, and applications, Chem. Soc. Rev. 45 (2016) 2327–2367, https://doi.org/10.1039/C5CS00837A.

[29] C.-S. Liu, Z.-H. Zhang, M. Chen, H. Zhao, F.-H. Duan, D.-M. Chen, M.-H. Wang, S. Zhang, M. Du, Pore modulation of zirconium–organic frameworks for high-efficiency detection of trace proteins, Chem. Commun. 53 (2017) 3941–3944, https://doi.org/10.1039/C7CC00029D.

[30] S. Palanisamy, D. Senthil Raja, B. Subramani, T.-H. Wu, Y.-M. Wang, Label-free bimetallic in situ-grown 3D nickel-foam-supported NH_2-MIL-88B(Fe_2Co)-MOF-based impedimetric immunosensor for the detection of cardiac troponin I, ACS Appl. Mater. Interfaces 12 (2020) 32468–32476, https://doi.org/10.1021/acsami.0c09086.

[31] H.-T. Zhang, J.-W. Zhang, G. Huang, Z.-Y. Du, H.-L. Jiang, An amine-functionalized metal–organic framework as a sensing platform for DNA detection, Chem. Commun. 50 (2014) 12069–12072, https://doi.org/10.1039/C4CC05571C.

[32] L. Feng, S. Yuan, J.-L. Li, K.-Y. Wang, G.S. Day, P. Zhang, Y. Wang, H.-C. Zhou, Uncovering two principles of multivariate hierarchical metal–organic framework synthesis via retrosynthetic design, ACS Cen. Sci. 4 (2018) 1719–1726, https://doi.org/10.1021/acscentsci.8b00722.

[33] F. Su, S. Zhang, H. Ji, H. Zhao, J.-Y. Tian, C.-S. Liu, Z. Zhang, S. Fang, X. Zhu, M. Du, Two-dimensional zirconium-based metal–organic framework nanosheet composites embedded with au nanoclusters: a highly sensitive electrochemical aptasensor toward detecting cocaine, ACS Sensors 2 (2017) 998–1005, https://doi.org/10.1021/acssensors.7b00268.

[34] M. Wang, M. Hu, Z. Li, L. He, Y. Song, Q. Jia, Z. Zhang, M. Du, Construction of Tb-MOF-on-Fe-MOF conjugate as a novel platform for ultrasensitive detection of carbohydrate antigen 125 and living cancer cells, Biosens. Bioelectron. 142 (2019), 111536, https://doi.org/10.1016/j.bios.2019.111536.

[35] L. Chen, H.-F. Wang, C. Li, Q. Xu, Bimetallic metal–organic frameworks and their derivatives, Chem. Sci. 11 (2020) 5369–5403, https://doi.org/10.1039/D0SC01432J.

[36] B. Iqbal, M. Saleem, S.N. Arshad, J. Rashid, N. Hussain, M. Zaheer, One-pot synthesis of heterobimetallic metal–organic frameworks (mofs) for multifunctional catalysis, Chem. Eur. J. 25 (2019) 10490–10498, https://doi.org/10.1002/chem.201901939.

[37] Y. Liu, C. Wang, S. Ju, M. Li, A. Yuan, G. Zhu, FeCo-based hybrid MOF derived active species for effective oxygen evolution, Prog. Nat. Sci. Mater. Inter. 30 (2020) 185–191, https://doi.org/10.1016/j.pnsc.2020.02.006.

[38] P. Yuan, N. Zhang, D. Zhang, T. Liu, L. Chen, X. Liu, R. Ma, G. Qiu, Fabrication of nickel-foam-supported layered zinc–cobalt hydroxide nanoflakes for high electrochemical performance in supercapacitors, Chem. Commun. 50 (2014) 11188–11191, https://doi.org/10.1039/C4CC05057F.

[39] M. Kundu, C.C.A. Ng, D.Y. Petrovykh, L. Liu, Nickel foam supported mesoporous MnO_2 nanosheet arrays with superior lithium storage performance, Chem. Commun. 49 (2013) 8459–8461, https://doi.org/10.1039/C3CC44079F.

[40] H. Wang, G. Wang, Y. Ling, F. Qian, Y. Song, X. Lu, S. Chen, Y. Tong, Y. Li, High power density microbial fuel cell with flexible 3D graphene–nickel foam as anode, Nanoscale 5 (2013) 10283–10290, https://doi.org/10.1039/C3NR03487A.

[41] L. Deng, S. Fan, Y. Chen, J. Chen, Z. Mai, Z. Xiao, In situ growing CuO/ZIF-8 into nickel foam to fabricate a binder-free self-supported glucose biosensor, Ind. Eng. Chem. Res. 61 (2022) 7312–7321, https://doi.org/10.1021/acs.iecr.2c01298.

[42] Y. Wan, D. Zhang, Y. Wang, B. Hou, A 3D-impedimetric immunosensor based on foam Ni for detection of sulfate-reducing bacteria, Electrochem. Commun. 12 (2) (2010) 288–291, https://doi.org/10.1016/j.elecom.2009.12.017.

[43] M. Amoretti, C. Amsler, G. Bonomi, A. Bouchta, P. Bowe, C. Carraro, C.L. Cesar, M. Charlton, M.J.T. Collier, M. Doser, V. Filippini, K.S. Fine, A. Fontana, M. C. Fujiwara, R. Funakoshi, P. Genova, J.S. Hangst, R.S. Hayano, M.H. Holzscheiter, L.V. Jørgensen, V. Lagomarsino, R. Landua, D. Lindelöf, E.L. Rizzini, M. Macrì, N. Madsen, G. Manuzio, M. Marchesotti, P. Montagna, H. Pruys, C. Regenfus, P. Riedler, J. Rochet, A. Rotondi, G. Rouleau, G. Testera, A. Variola, T.L. Watson, D.P. van der Werf, Production and detection of cold antihydrogen atoms, Nature 419 (2002) 456–459, https://doi.org/10.1038/nature01096.

[44] C. Yuan, L. Yang, L. Hou, L. Shen, X. Zhang, X.W. Lou, Growth of ultrathin mesoporous Co_3O_4 nanosheet arrays on Ni foam for high-performance electrochemical capacitors, Energ. Environ. Sci. 5 (2012) 7883–7887, https://doi.org/10.1039/C2EE21745G.
[45] G. Zhang, X.W. Lou, General solution growth of mesoporous $NiCo_2O_4$ nanosheets on various conductive substrates as high-performance electrodes for supercapacitors, Adv. Mater. 25 (2013) 976–979, https://doi.org/10.1002/adma.201204128.
[46] Q. Wang, J. Lu, Y. Jiang, S. Yang, Y. Yang, Z. Wang, FeCo bimetallic metal organic framework nanosheets as peroxymonosulfate activator for selective oxidation of organic pollutants, Chem. Eng. J. 443 (2022), 136483, https://doi.org/10.1016/j.cej.2022.136483.
[47] X. Zhao, B. Pattengale, D. Fan, Z. Zou, Y. Zhao, J. Du, J. Huang, C. Xu, Mixed-node metal–organic frameworks as efficient electrocatalysts for oxygen evolution reaction, ACS Energy Lett. 3 (2018) 2520–2526, https://doi.org/10.1021/acsenergylett.8b01540.
[48] J. Tian, F. Jiang, D. Yuan, L. Zhang, Q. Chen, M. Hong, Electric-field assisted in situ hydrolysis of bulk metal–organic frameworks (MOFs) into ultrathin metal oxyhydroxide nanosheets for efficient oxygen evolution, Angew. Chem. 59 (2020) 13101–13108, https://doi.org/10.1002/anie.202004420.
[49] S. Kumar, S. Kumar, S. Tiwari, S. Srivastava, M. Srivastava, B.K. Yadav, S. Kumar, T.T. Tran, A.K. Dewan, A. Mulchandani, J.G. Sharma, S. Maji, B.D. Malhotra, Biofunctionalized nanostructured zirconia for biomedical application: a smart approach for oral cancer detection, Adv. Sci. 2 (2015) 1500048, https://doi.org/10.1002/advs.201500048.
[50] J. Chen, J. Zhang, Y. Guo, J. Li, F. Fu, H.-H. Yang, G. Chen, An ultrasensitive electrochemical biosensor for detection of DNA species related to oral cancer based on nuclease-assisted target recycling and amplification of DNAzyme, Chem. Commun. 47 (2011) 8004–8006, https://doi.org/10.1039/C1CC11929J.
[51] R. Malhotra, V. Patel, J.P. Vaqué, J.S. Gutkind, J.F. Rusling, Ultrasensitive electrochemical immunosensor for oral cancer biomarker IL-6 using carbon nanotube forest electrodes and multilabel amplification, Anal. Chem. 82 (2010) 3118–3123, https://doi.org/10.1021/ac902802b.
[52] S. Viswanathan, C. Rani, A. Vijay Anand, J.-A. Ho, Disposable electrochemical immunosensor for carcinoembryonic antigen using ferrocene liposomes and MWCNT screen-printed electrode, Biosens. Bioelectron. 24 (7) (2009) 1984–1989.
[53] L. Boldrup, P. Coates, X. Gu, L. Wang, R. Fåhraeus, T. Wilms, N. Sgaramella, K. Nylander, Low potential of circulating interleukin 1 receptor antagonist as a prediction marker for squamous cell carcinoma of the head and neck, J. Oral Pathol. Med. 50 (2021) 785–794, https://doi.org/10.1111/jop.13187.

Hierarchical ensembles of FeCo metal-organic frameworks reinforced nickel foam as an impedimetric sensor for detection of IL-1RA in human samples

原創性報告

24%	17%	21%	5%
相似度指數	網際網絡來源	出版物	學生文稿

主要來源

1	www.mdpi.com 網際網絡來源	2%
2	Sathyadevi Palanisamy, Duraisamy Senthil Raja, Boopathi Subramani, Tung-Ho Wu, Yun-Ming Wang. " Label-Free Bimetallic In Situ-Grown 3D Nickel-Foam-Supported NH -MIL-88B(Fe Co)-MOF-based Impedimetric Immunosensor for the Detection of Cardiac Troponin I ", ACS Applied Materials & Interfaces, 2020 出版物	2%
3	www.researchgate.net 網際網絡來源	1%
4	eprints.whiterose.ac.uk 網際網絡來源	1%
5	Shilpi Verma, Anu Singh, Ajay Shukla, Jyoti Kaswan, Kavita Arora, Jaime Ramirez-Vick, Priti Singh, Surinder P. Singh. "Anti-IL8/AuNPs-rGO/ITO as an Immunosensing Platform for	1%

Noninvasive Electrochemical Detection of Oral Cancer", ACS Applied Materials & Interfaces, 2017
出版物

6	pubs.rsc.org 網際網絡來源	1 %
7	Zhenghan Shi, Yanli Lu, Zetao Chen, Chen Cheng, Jie Xu, Qingqing Zhang, Zupeng Yan, Zisheng Luo, Qingjun Liu. "Electrochemical non-enzymatic sensing of glycoside toxins by boronic acid functionalized nano-composites on screen-printed electrode", Sensors and Actuators B: Chemical, 2020 出版物	1 %
8	dspace.lib.cranfield.ac.uk 網際網絡來源	1 %
9	Sathyadevi Palanisamy, Hsu-Min Wu, Li-Yun Lee, Shyng-Shiou F. Yuan, Yun-Ming Wang. "Fabrication of 3D Amino-Functionalized Metal–Organic Framework on Porous Nickel Foam Skeleton to Combinate Follicle Stimulating Hormone Antibody for Specific Recognition of Follicle-Stimulating Hormone", JACS Au, 2021 出版物	1 %
10	dokumen.pub 網際網絡來源	1 %

11	pubmed.ncbi.nlm.nih.gov 網際網絡來源	1 %
12	www.rsc.org 網際網絡來源	1 %
13	link.springer.com 網際網絡來源	<1 %
14	www.nature.com 網際網絡來源	<1 %
15	Yao-Chen Chuang, Yi-Po Chen, Hsu-Min Wu, Jui-Sheng Hsu, Leu-Wei Lo, Yun-Ming Wang. "Matrix metalloproteinase-directed precise targeting and smart drug delivery of biodegradable gold nanodandelions as CT imaging guided anticancer therapy", Journal of Drug Delivery Science and Technology, 2022 出版物	<1 %
16	Sathyadevi Palanisamy, Duraisamy Senthil Raja, Boopathi Subramani, Tung-Ho Wu, Yun-Ming Wang. "Label-Free Bimetallic In Situ Grown 3D Nickel Foam Supported NH2-MIL-88B(Fe2Co)-MOF based Impedimetric Immunosensor for the Detection of Cardiac Troponin I", ACS Applied Materials & Interfaces, 2020 出版物	<1 %

17	Submitted to University of New South Wales 學生文稿	<1 %
18	www.pubfacts.com 網際網絡來源	<1 %
19	Submitted to Taipei Medical University 學生文稿	<1 %
20	Zdeněk Farka, Tomáš Juřík, David Kovář, Libuše Trnková, Petr Skládal. "Nanoparticle-Based Immunochemical Biosensors and Assays: Recent Advances and Challenges", Chemical Reviews, 2017 出版物	<1 %
21	coek.info 網際網絡來源	<1 %
22	Submitted to University of Southampton 學生文稿	<1 %
23	www.coudert.name 網際網絡來源	<1 %
24	www.tandfonline.com 網際網絡來源	<1 %
25	Submitted to University of Strathclyde 學生文稿	<1 %
26	Maite Domínguez-Fernández, Iziar A. Ludwig, María-Paz De Peña, Concepción Cid. " Bioaccessibility of Tudela artichoke (cv.	<1 %

Blanca de Tudela) (poly)phenols: the effects of heat treatment, simulated gastrointestinal digestion and human colonic microbiota ", Food & Function, 2021
出版物

27	przyrbwn.icm.edu.pl 網際網絡來源	<1%
28	pub.epsilon.slu.se 網際網絡來源	<1%
29	bioresources.cnr.ncsu.edu 網際網絡來源	<1%
30	doaj.org 網際網絡來源	<1%
31	Submitted to Indian School of Mines 學生文稿	<1%
32	clausiuspress.com 網際網絡來源	<1%
33	Chong Cheng, Shuang Li, Arne Thomas, Nicholas A. Kotov, Rainer Haag. "Functional Graphene Nanomaterials Based Architectures: Biointeractions, Fabrications, and Emerging Biological Applications", Chemical Reviews, 2017 出版物	<1%
34	Mucian Lee, Sathyadevi Palanisamy, Bin-Hou Zhou, Li-Yu Wang, Chiao-Yun Chen, Chen-Yi	<1%

Lee, Shyng-Shiou F. Yuan, Yun-Ming Wang. "Ultrasensitive Electrical Detection of Follicle-Stimulating Hormone Using a Functionalized Silicon Nanowire Transistor Chemosensor", ACS Applied Materials & Interfaces, 2018
出版物

---

35 Ruchika Malhotra, Vyomesh Patel, Jose Pedro Vaqué, J. Silvio Gutkind, James F. Rusling. "Ultrasensitive Electrochemical Immunosensor for Oral Cancer Biomarker IL-6 Using Carbon Nanotube Forest Electrodes and Multilabel Amplification", Analytical Chemistry, 2010 <1%
出版物

---

36 Peng Qi. "Reduced Graphene Sheets Modified Electrodes for Electrochemical Detection of Sulfide", Electroanalysis, 12/2011 <1%
出版物

---

37 Xinbo Pan, Haitao Xu, Xi Zhao, Huaqian Zhang. " Metal–Organic Framework-Membranized Bicomponent Core–Shell Catalyst HZSM-5@UIO-66-NH /Pd for CO Selective Conversion ", ACS Sustainable Chemistry & Engineering, 2019 <1%
出版物

---

38 eprints.qut.edu.au <1%
網際網絡來源

---

patents.google.com

39	網際網絡來源	<1%
40	www.spandidos-publications.com 網際網絡來源	<1%
41	Dhanaprabhu Pattappan, Amirthalingam Mohankumar, R.T. Rajendra Kumar, Sundararaj Palanisamy et al. "Visible light photocatalytic activity of a FeCo metal-organic framework for degradation of acetaminophen and 2,4-dichlorophenoxyacetic acid and a nematode-based ecological assessment", Chemical Engineering Journal, 2023 出版物	<1%
42	Kai Wen, Xingdong Yang, Cuiling Zhang, Huiying Wei, Guizheng Zou, Ye Zhu. "Exonuclease III-assisted positive feedback signal amplification strategy for ultrasensitive electrochemical detection of nucleic acids", Sensors and Actuators B: Chemical, 2019 出版物	<1%
43	www.siftdesk.org 網際網絡來源	<1%
44	Deepshikha Shahdeo, Sonu Gandhi. "Next generation biosensors as a cancer diagnostic tool", Elsevier BV, 2022 出版物	<1%

45	Shilpi Verma, Surinder P. Singh. "Non-invasive oral cancer detection from saliva using zinc oxide–reduced graphene oxide nanocomposite based bioelectrode", MRS Communications, 2019 出版物	<1 %
46	Yi-Yu Zhang, Ling-Xuan Qian, Xing-Zhao Liu. "Determination of the Band Alignment of a-IGZO/a-IGMO Heterojunction for High-Electron Mobility Transistor Application", physica status solidi (RRL) - Rapid Research Letters, 2017 出版物	<1 %
47	Ying Zhang, Xiaocui Huang, Fang Luo, Yun Lei, Li Chen, Zuquan Weng, Longhua Guo, Zhenyu Lin. "Highly sensitive electrochemical immunosensor for golgi protein 73 based on proximity ligation assay and enzyme-powered recycling amplification", Analytica Chimica Acta, 2018 出版物	<1 %
48	docksci.com 網際網絡來源	<1 %
49	dspace.ncl.res.in:8080 網際網絡來源	<1 %
50	oak.jejunu.ac.kr 網際網絡來源	<1 %

51	ris.utwente.nl 網際網絡來源	<1 %
52	titula.universidadeuropea.es 網際網絡來源	<1 %
53	www.journal-aquaticscience.com 網際網絡來源	<1 %
54	Duraisamy Senthil Raja, Chun-Lung Huang, Yu-An Chen, YongMan Choi, Shih-Yuan Lu. "Composition-balanced trimetallic MOFs as ultra-efficient electrocatalysts for oxygen evolution reaction at high current densities", Applied Catalysis B: Environmental, 2020 出版物	<1 %
55	Elif Burcu Aydın, Mustafa Kemal Sezgintürk. "A disposable and ultrasensitive ITO based biosensor modified by 6-phosphonohexanoic acid for electrochemical sensing of IL-1β in human serum and saliva", Analytica Chimica Acta, 2018 出版物	<1 %
56	Handbook of Nanoelectrochemistry, 2016. 出版物	<1 %
57	Lihong He, Fan Ping, Zhaona Fan, Chi Zhang, Miao Deng, Bin Cheng, Juan Xia. "Salivary exosomal miR-24-3p serves as a potential detective biomarker for oral squamous cell	<1 %

carcinoma screening", Biomedicine & Pharmacotherapy, 2020
出版物

58	Muhammad Anwar, Weijun Yu, Hong Yao, Ping Zhou, Andrew C. Allan, Lihui Zeng. "NtMYB3, an R2R3-MYB from Narcissus, Regulates Flavonoid Biosynthesis", International Journal of Molecular Sciences, 2019 出版物	<1 %
59	Namrata Pachauri, Kashyap Dave, Amit Dinda, Pratima R. Solanki. " Cubic CeO implanted reduced graphene oxide-based highly sensitive biosensor for non-invasive oral cancer biomarker detection ", Journal of Materials Chemistry B, 2018 出版物	<1 %
60	accedacris.ulpgc.es 網際網絡來源	<1 %
61	citeseerx.ist.psu.edu 網際網絡來源	<1 %
62	core-cms.prod.aop.cambridge.org 網際網絡來源	<1 %
63	dspace.jaist.ac.jp 網際網絡來源	<1 %
64	worldwidescience.org 網際網絡來源	<1 %

65	www.freepatentsonline.com 網際網絡來源	<1%
66	Cai, Daoping, Hui Huang, Dandan Wang, Bin Liu, Lingling Wang, Yuan Liu, Qiuhong Li, and Taihong Wang. "High-performance Supercapacitor Electrode Based on the Unique ZnO@Co3O4 Core/shell Hetero-structures on Nickel Foam", ACS Applied Materials & Interfaces 出版物	<1%
67	L. Han, J. Xu, X. Zhu, F. Yang, X. Jia. "High-performance Ni-V-Fe metal-organic framework electrocatalyst composed of integrated nanowires and nanosheets for oxygen evolution reaction", Materials Today Energy, 2020 出版物	<1%
68	Meenakshi Choudhary, Prashant Yadav, Anu Singh, Satbir Kaur et al. "CD 59 Targeted Ultrasensitive Electrochemical Immunosensor for Fast and Noninvasive Diagnosis of Oral Cancer", Electroanalysis, 2016 出版物	<1%
69	Mi Wu, Qiangshun Wu, Yuankun Yang, Zuming He, Hanpei Yang. "Regulating Lewis acidity and local electron density of iron-based metal organic frameworks via cerium doping for	<1%

efficient photo-Fenton process", Journal of Colloid and Interface Science, 2023
出版物

---

70 Minghua Wang, Bin Hu, Hongfei Ji, Yingpan Song, Jiameng Liu, Donglai Peng, Linghao He, Zhihong Zhang. " Aptasensor Based on Hierarchical Core–Shell Nanocomposites of Zirconium Hexacyanoferrate Nanoparticles and Mesoporous mFe O @mC: Electrochemical Quantitation of Epithelial Tumor Marker Mucin-1 ", ACS Omega, 2017 <1%
出版物

---

71 Submitted to New Mexico State University <1%
學生文稿

---

72 Smriti Sri, G.B.V.S. Lakshmi, Payal Gulati, Deepika Chauhan, Alok Thakkar, Pratima R. Solanki. "Simple and facile carbon dots based electrochemical biosensor for TNF-α targeting in cancer patient's sample", Analytica Chimica Acta, 2021 <1%
出版物

---

73 Walcarius, Alain. "Mesoporous Materials-Based Electrochemical Sensors", Electroanalysis, 2015. <1%
出版物

---

74 Yu Li, Changbao Wang, Zhenzhen Li, Minghua Wang, Linghao He, Zhihong Zhang. "Zirconium-porphyrin complex as novel <1%

nanocarrier for label-free impedimetric biosensing neuron-specific enolase", Sensors and Actuators B: Chemical, 2020
出版物

75	archive.org 網際網絡來源	<1%
76	dspace.dtu.ac.in:8080 網際網絡來源	<1%
77	electrochemsci.org 網際網絡來源	<1%
78	onlinelibrary.wiley.com 網際網絡來源	<1%
79	www.cell.com 網際網絡來源	<1%
80	www.frontiersin.org 網際網絡來源	<1%
81	www.oncotarget.com 網際網絡來源	<1%
82	Jasmeen Kaur, Rohit Srivastava, Vivek Borse. "Recent advances in point-of-care diagnostics for oral cancer", Biosensors and Bioelectronics, 2021 出版物	<1%
83	Jitendra N. Tiwari, Varun Vij, K. Christian Kemp, Kwang S. Kim. "Engineered Carbon-	<1%

Nanomaterial-Based Electrochemical Sensors for Biomolecules", ACS Nano, 2015
出版物

---

84 Masashi Shiiba, Kengo Saito, Hitomi Yamagami, Dai Nakashima, Morihiro Higo, Atsushi Kasamatsu, Yosuke Sakamoto, Katsunori Ogawara, Katsuhiro Uzawa, Yuichi Takiguchi, Hideki Tanzawa. "Interleukin-1 receptor antagonist (IL1RN) is associated with suppression of early carcinogenic events in human oral malignancies", International Journal of Oncology, 2015 <1%
出版物

---

85 William P Arend. "The balance between IL-1 and IL-1Ra in disease", Cytokine & Growth Factor Reviews, 2002 <1%
出版物

---

86 Amber M. Bates, Maria Paula Gomez Hernandez, Emily A. Lanzel, Fang Qian, Kim A. Brogden. "Matrix metalloproteinase (MMP) and immunosuppressive biomarker profiles of seven head and neck squamous cell carcinoma (HNSCC) cell lines", Translational Cancer Research, 2018 <1%
出版物

---

87 Xiaolin Huang, Yijing Liu, Bryant Yung, Yonghua Xiong, Xiaoyuan Chen. " Nanotechnology-Enhanced No-Wash <1%

Biosensors for Diagnostics of Cancer ", ACS Nano, 2017
出版物

88 Yuanjing Cui, Yanfeng Yue, Guodong Qian, Banglin Chen. "Luminescent Functional Metal –Organic Frameworks", Chemical Reviews, 2011 <1%
出版物

排除引述	開	排除相符處	關閉
排除參考書目	開		